

A Frequency-Shift Method to Measure Shear-Wave Attenuation in Soft Tissues

Simon Bernard, Siavash Kazemirad, and Guy Cloutier, *Senior Member, IEEE*

Abstract—*In vivo* quantification of shear-wave attenuation in soft tissues may help to better understand human tissue rheology and lead to new diagnostic strategies. Attenuation is difficult to measure in acoustic radiation force elastography because the shear-wave amplitude decreases due to a combination of diffraction and viscous attenuation. Diffraction correction requires assuming a cylindrical wavefront and an isotropic propagation medium, which may not be the case in some applications. In this paper, the frequency-shift method, used in ultrasound imaging and seismology, was adapted for shear-wave attenuation measurement in elastography. This method is not sensitive to diffraction effects. For a linear frequency dependence of the attenuation, a closed-form relation was obtained between the decrease in the peak frequency of the gamma-distributed wave amplitude spectrum and the attenuation coefficient of the propagation medium. The proposed method was tested against a plane-wave reference method in homogeneous agar-gelatin phantoms with 0%, 10%, and 20% oil concentrations, and hence different attenuations of 0.117, 0.202, and 0.292 $\text{Np} \cdot \text{m}^{-1}/\text{Hz}$, respectively. Applicability to biological tissues was demonstrated with two *ex vivo* porcine liver samples (0.79 and 1.35 $\text{Np} \cdot \text{m}^{-1}/\text{Hz}$) and an *in vivo* human muscle, measured along (0.43 $\text{Np} \cdot \text{m}^{-1}/\text{Hz}$) and across (1.77 $\text{Np} \cdot \text{m}^{-1}/\text{Hz}$) the tissue fibers. In all cases, the data supported the assumptions of a gamma-distributed spectrum for the source and linear frequency attenuation for the tissue. This method provides tissue attenuation, which is relevant diagnostic information to model viscosity, in addition to shear-wave velocity used to assess elasticity. Data processing is simple and could be performed automatically in real time for clinical applications.

Index Terms—Attenuation, elastography, liver, muscle, rheology, spectral shift, viscoelasticity.

I. INTRODUCTION

ELASTOGRAPHY aims at measuring the stiffness of biological tissues noninvasively. Tissue stiffness not only varies greatly between different biological tissues, as reviewed in [1] and [2], but is also modified by pathologies. Recently,

Manuscript received April 22, 2016; accepted November 25, 2016. Date of publication December 1, 2016; date of current version March 1, 2017. The work of S. Bernard was supported by a MÉDITIS post-doctoral fellowship of the Natural Sciences and Engineering Research Council of Canada provided by the Institute of Biomedical Engineering of the École Polytechnique and University of Montréal. The work of S. Kazemirad was supported by a post-doctoral fellowship award of the Fonds de Recherche du Québec - Nature et Technologies under Award FRQNT #184900. This work was supported by FRQNT under Grant #PR-174387.

S. Bernard and S. Kazemirad are with the Laboratory of Biorheology and Medical Ultrasonics, University of Montréal Hospital Research Center, Montréal, QC H2X OA9, Canada.

G. Cloutier is with the Laboratory of Biorheology and Medical Ultrasonics, University of Montréal Hospital Research Center, Montréal, QC H2X OA9, Canada, and also with the Department of Radiology, Radio-Oncology and Nuclear Medicine, and the Institute of Biomedical Engineering, University of Montréal, Montréal, QC H3C 3J7, Canada (e-mail: guy.cloutier@umontreal.ca).

Digital Object Identifier 10.1109/TUFFC.2016.2634329

elastography has been shown to provide relevant diagnostic information in clinical applications such as breast cancer [3] and liver fibrosis [4].

As stiffness relates the applied stress to the induced tissue motion, all elastography methods rely on a measurement of the tissue motion, which is usually performed using magnetic resonance (MR) or ultrasound (US) imaging. The stress at the origin of the motion can either be (quasi-)static or dynamic, and induced by physiological motion [5], an external source [6], or acoustic radiation force [2], [7]–[9]. Dynamic elastography methods rely on elastic wave propagation to estimate stiffness. In a purely elastic and incompressible medium, the propagation speed c of a shear wave is directly related to the Young modulus E and mass density ρ through the relation $E = 3\rho c^2$.

However, all biological tissues are viscoelastic to some extent, which entails wave dispersion (frequency dependence of the velocity) and attenuation [10]. Tissue viscosity has received much less attention than elasticity in elastography studies, although there is a growing set of evidences that viscoelasticity-related parameters may improve diagnosis. In MR elastography, a significant difference in wave attenuation was observed between healthy and diseased muscles [11], and an increase in loss modulus was found to be a better discriminator than a rise in shear storage modulus to separate benign and malignant liver tumors [12]. The shear storage and loss moduli are the real and imaginary parts of the complex shear modulus, respectively. The loss modulus is related to the amount of energy dissipated through viscous damping. Alternatively, with quasi-static US elastography, viscoelasticity assessment was found to improve the discrimination of benign and malignant breast tumors [13].

In radiation force US elastography, studies have proposed to use the shear-wave speed dispersion to estimate viscosity [14]–[16], through the assumption of a rheological model for the tissue (usually a Voigt model). A more direct way to assess viscosity is the measurement of shear-wave attenuation, which has been hindered by technical difficulties. Indeed, both viscoelastic attenuation and geometrical spreading of the wave energy (diffraction) generally affect the wave amplitude over propagation distance. These two effects cannot be separated without the use of numerical simulations [6] or strong geometrical assumptions (e.g., cylindrical spreading of the waves). Two methods based on such assumption have recently been proposed [17], [18]. Nenadic *et al.* [17] suggested the use of a 2-D Fourier transform: the maximum of the frequency–wavenumber spectrum at each frequency is related to the wave speed $c(f)$, while its width is related to

the attenuation $\alpha(f)$. The theoretical development associated with that method is given in [19]. It is shown that the equation relating attenuation and spectral width is, however, dependent on the geometry of the wavefront, and cylindrical spreading of the wave was therefore assumed in [17]. Kazemirad *et al.* [18] proposed a straightforward approach in which the decay in shear-wave amplitude versus propagation distance was corrected before estimating the viscosity, by considering a cylindrical shear wavefront produced by the source. The two methods therefore share the same geometrical assumption, but differ in the way they process the data (in the frequency–wavenumber space for [17] and in the frequency–propagation distance space for [18]).

Although promising results were obtained, these two latter methods share limitations related to the assumption of a cylindrical wavefront. The radiation force source generated by linear US probes is neither infinitely long in the depth direction nor perfectly cylindrical due to different focus properties in the lateral and elevation directions. This asymmetry generates waves that decrease in amplitude at a slower rate than purely cylindrical waves [19]. Although this source of bias might be corrected for by taking into account the exact source geometry, it would require advanced modeling and likely be both probe and depth dependent. Moreover, many soft tissues are anisotropic, like muscles [14], [20], tendons [21], and kidneys [22]. In such tissues, the wave generated by a line source is not cylindrical [23], [24] due to a direction-dependent velocity, which may likely induce a tissue-dependent bias in attenuation. A measurement method that does not rely on the cylindrical wave assumption is therefore of interest.

In the areas of seismology and medical US imaging, researchers have been interested in wave attenuation for decades. A popular measurement method in both fields is the frequency-shift method. This method is based on the change in the frequency content of the wave as it travels through an attenuating medium, due to stronger attenuation at higher frequencies. Since it is not based on the absolute amplitude of the wave, but only on relative magnitudes of the different frequency components, this method is less sensitive to geometrical spreading of the wave. In US imaging, this method was born in the late 1970s/early 1980s [25]–[27], and a modern presentation was given in [28]. In geophysics, the frequency-shift method has been applied to seismic waves [29] and electromagnetic waves [30], and was combined to tomographic principles to provide attenuation maps.

Although the frequency dependence of shear-wave attenuation in soft tissues has already been reported, it has been mostly considered as a drawback limiting the precision of velocity measurements at high frequencies due to reduced signal-to-noise ratios [6], [14]. This phenomenon was used in this paper for quantitative estimation of the shear-wave attenuation. First, the theory associated with the frequency-shift method is presented and adapted to elastography. Then, the application of the proposed method to *in vitro* phantoms, *ex vivo* liver tissues, and an *in vivo* muscle tissue is described. For evaluation purposes, phantom measurements were also performed by a plane-wave transmission method to provide reference measures. The validity

of the hypotheses and implication of the results are then discussed.

II. THEORY

The theory associated with the frequency-shift method as it is applied in seismology and US imaging is briefly presented here. For a more in-depth presentation, the reader is referred to [29]. Then, a new hypothesis on the amplitude spectral distribution is introduced to accurately describe the shear waves generated by US radiation force pushes, leading to a new frequency-shift equation for use in dynamic shear-wave elastography.

Let assume a 1-D shear wave propagating along the x -direction, whose spectrum is $S(f)$ at a point x_0 (not necessarily the position of the source). After propagation over a distance $\Delta x = x - x_0$, the spectrum measured at x is

$$|R(f)| = G(f, x) \cdot H(f, \Delta x) \cdot |S(f)| \quad (1)$$

where $G(f, x)$ describes geometrical effects and $H(f, \Delta x)$ corresponds to the viscous attenuation effect on the amplitude. Although viscoelasticity also affects both the phase (dispersion) and amplitude (attenuation) of propagating shear waves, the present method focusses only on attenuation and ignores the phase. The frequency-shift method first assumes that geometrical effects are independent of the frequency, i.e., $G(f, x) = G(x)$. Then, in geophysical and medical US applications, the attenuation is commonly supposed to depend linearly on frequency

$$H(f, \Delta x) = \exp(-\alpha_0 f \Delta x) \quad (2)$$

where α_0 is the (linear) attenuation coefficient. Finally, the amplitude spectrum produced by the source $|S(f)|$ is assumed to be normally distributed (Gaussian spectrum) in those applications, with a central frequency f_s and a variance σ^2

$$|S(f)| \propto \exp\left(-\frac{(f - f_s)^2}{\sigma^2}\right). \quad (3)$$

Under these hypotheses, the spectrum $|R(f)|$ after propagation is still Gaussian with a variance σ^2 and a central frequency given by [29]

$$f_r = f_s - \sigma^2 \alpha_0 \Delta x. \quad (4)$$

Hence, the attenuation coefficient can be deduced from the measurement of the central frequency at two or more positions along the propagation path.

For applications in shear-wave elastography, we keep the hypothesis of frequency-independent geometrical spreading and linear frequency-dependent attenuation. However, we use a different spectral distribution for the wave amplitude. As it will be illustrated later, the amplitude spectrum of the shear waves generated with a radiation force, in our experiments on phantoms and biological tissues, was not Gaussian but much better fitted by a gamma distribution

$$|S(f)| \propto f^{k_0-1} \cdot \exp(-f\beta_0) \quad (5)$$

where k_0 and β_0 are, respectively, the shape and rate parameters. In that case, the spectrum after propagation becomes

$$|R(f)| \propto G(x) \cdot \exp(-\alpha_0 f \Delta x) \cdot f^{k_0-1} \cdot \exp(-f\beta_0) \quad (6)$$

which simplifies to

$$|R(f)| \propto f^{k_0-1} \cdot \exp[-f(\beta_0 + \alpha_0 \Delta x)]. \quad (7)$$

The geometrical term $G(x)$ has been dropped since it is frequency independent and thus does not affect the spectral distribution of the amplitude. Equation (7) still describes a gamma distribution with an unchanged shape parameter k_0 and a new rate parameter

$$\beta(\Delta x) = \beta_0 + \alpha_0 \Delta x. \quad (8)$$

If the spectrum of the shear wave is measured at several positions along its propagation path, the attenuation coefficient α_0 can be estimated as the slope of the varying rate parameter $\beta(\Delta x)$, which can itself be obtained from a gamma fit of the spectrum at each position. The mean frequency f_m and peak frequency f_p (modes of the gamma distribution) are

$$f_m = k_0/\beta \quad (9)$$

$$f_p = (k_0 - 1)/\beta, \text{ for } k_0 > 1 \quad (10)$$

which are both inversely proportional to the rate parameter β . Equations (7), (8), and (10) form the basis of a frequency-shift method for a gamma-distributed amplitude spectrum and a linear attenuation medium. The validity of the hypotheses (linear attenuation and gamma-distributed spectrum) is discussed later in the light of the experimental data.

III. EXPERIMENTS

A. Preparation of Phantoms

Three phantoms were prepared with a mixture of 5% agar (A9799, Sigma–Aldrich chemical, St Louis, MO, USA), 4% gelatine (G2500, Sigma–Aldrich chemical), and a varying percentage of castor oil (259853, Sigma–Aldrich chemical). Castor oil concentrations of 0%, 10%, and 20% were used to vary the viscosity of the phantoms, and thus wave attenuation. A small quantity of glucosamine (0.2%) was also added to the 10% and 20% oil phantoms to stabilize the emulsion and avoid the separation of water and castor oil [31]. Gelatin was first dissolved in water at 90 °C. Then, glucosamine and castor oil were added. After cooling down to 50 °C, agar powder was added. At this temperature, agar particles did not dissolve and therefore provided a speckle pattern in US images of phantoms. The mixture was further cooled down to room temperature (about 23 °C) and casted in a $20 \times 10 \times 10$ cm³ rectangular mold. An 8×10 cm² rectangular Plexiglas plate was inserted within the mixture before gelification for reference plane-wave attenuation measurements (Section III-C). The phantoms were stored in a refrigerator at 4 °C for about 18 h overnight, and placed at room temperature 6 h before measurements.

B. Frequency-Shift Measurements

For the frequency-shift method, shear waves were generated using a sequence composed of three successive 125- μ s-long radiation force pushes, focused at the center of the US probe at depths of 20, 25, and 30 mm (Fig. 1), similarly to SuperSonic imaging [9]. The probe (ATL L7-4 Philips, Bothell, WA, USA) was used at its 5-MHz

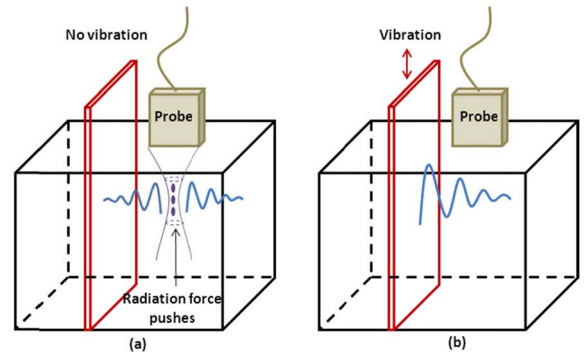


Fig. 1. Setup for the phantom measurements. (a) For the frequency-shift method, displacements were generated by three radiation force pushes. The wave amplitude decreased over distance due to viscoelastic attenuation and geometrical spreading. (b) For the reference method, vibration of the plate induced a plane wave, whose amplitude decreased due to the sole effect of phantom viscoelasticity.

central frequency, and was driven by a research US system (V1, Verasonics Inc., Redmond, WA, USA). A similar sequence generated by the same setup was found to lie within the acceptable range of mechanical index and intensity suggested by the U.S. Food and Drug Administration for *in vivo* applications [32].

Immediately after the generation of the pushes, the same probe was used to image the medium with plane-wave imaging at a 4-kHz frame rate, during 20 ms. The plane-wave RF data were beamformed using a Fourier domain method [33]. The interframe axial displacement field [i.e., the particle velocity field $v(x, z, t)$] was then estimated with a conventional 1-D normalized cross-correlation algorithm [34]. No passband filtering was applied to preserve the shape of the amplitude spectrum. No time–space directional filtering [35], [36] was also required, due to the use of a single shear-wave source orthogonal to the probe lateral direction and because of the homogeneity of most investigated media. Each experiment was repeated ten times in a very short time lapse (less than 500 ms overall) with yet enough time for the shear-wave field to completely vanish in the observed domain between successive acquisitions. The velocity field was averaged over this set of experiments to decrease the impact of random noise. A snapshot of the particle velocity field about 1 ms after the pushing sequence obtained for the 0% oil phantom is pictured in Fig. 2(a). The particle velocity was on the order of a few millimeters/second, corresponding to displacement amplitudes on the order of a few micrometers, which is typical of acoustic radiation force experiments in soft tissues [9], [14].

Similarly to what was done in [14], the 2-D particle velocity field $v(x, z, t)$ was averaged along the depth dimension z over a height h , centered on the midpush position ($z = 25$ mm). Then, the mean of time profiles obtained at each lateral position x [three of them are presented in Fig. 2(b)–(d)] was removed before Fourier transform to get the experimental amplitude spectrum $|\hat{S}(f, \Delta x)|$ as a function of the propagation distance. Three spectra obtained respectively at locations 5, 10, and 15 mm away from the pushing line, are plotted in Fig. 2(e). It can be observed that these spectra are asymmetric, with a longer tail on the high-frequency side, and cannot be described by a Gaussian distribution. The 4-kHz sampling

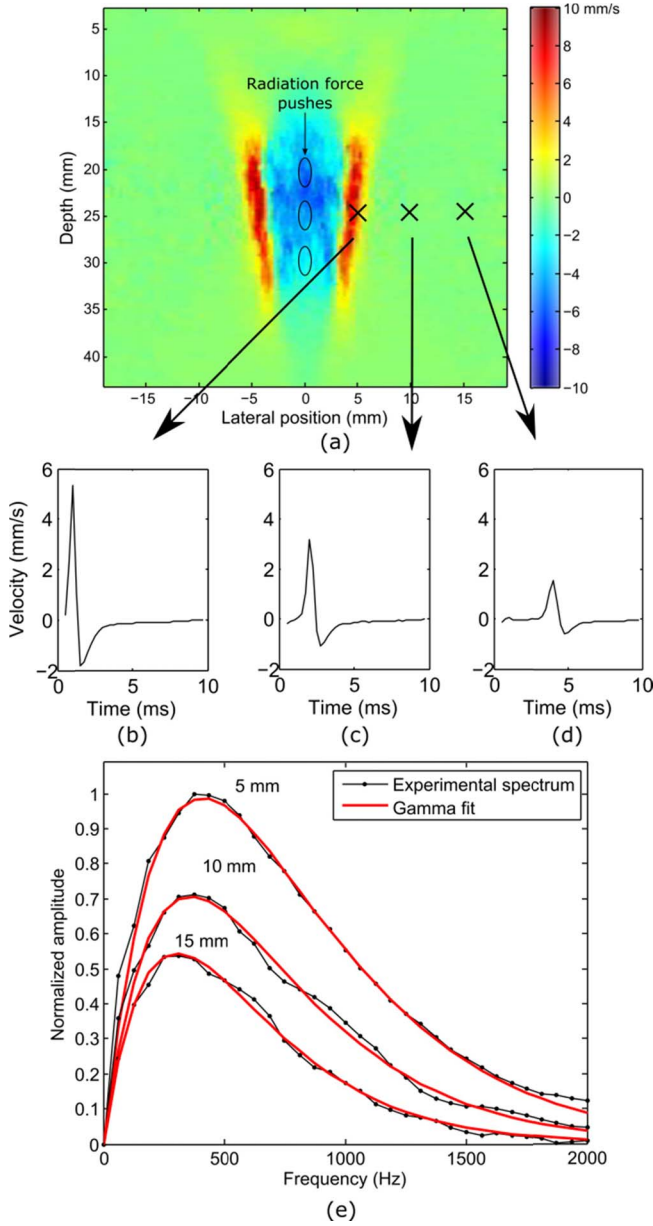


Fig. 2. (a) Particle velocity field 1 ms after the generation of the radiation force pushes at depths of 20, 25, and 30 mm. (b)–(d) Time profiles recorded at the three highlighted lateral positions of 5, 10, and 15 mm are plotted. (e) Amplitude spectra of these time signals are plotted with their gamma distribution fitted curves.

rate was sufficient as the wave amplitude rapidly decreased at high frequencies. The frequency resolution of the spectra was sufficient without requiring zero padding of the time domain signals.

At a given distance x_0 away from the pushing line, a nonlinear least-square algorithm (Levenberg–Marquardt) was used to estimate the three parameters A_0 , k_0 , and β_0 of the gamma distribution, as

$$\{A_0, k_0, \beta_0\} = \underset{A, k, \beta}{\operatorname{argmin}} [|\hat{S}(f, x_0)| - Af^{k-1} \cdot \exp(-f\beta)]^2 \quad (11)$$

where A is an amplitude parameter necessary to account for the *a priori* unknown scale of the measured data. According to the theory developed in Section II, under the hypothesis

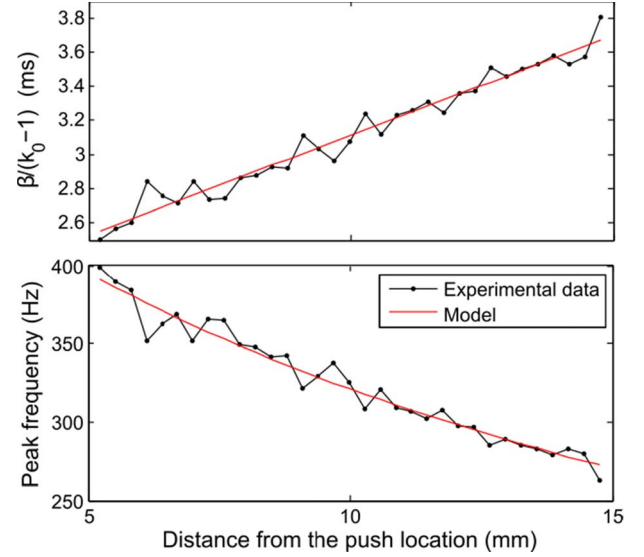


Fig. 3. Rate parameter of the wave amplitude spectrum (top) and peak frequency (bottom, inverse of the top curve) versus propagation distance. After fitting of the attenuation coefficient, the model based on a linear attenuation hypothesis accurately describes the observed frequency shift.

of linear attenuation, the spectrum at a position Δx further away from the pushing line can be described by a gamma distribution whose k_0 is similar to that at x_0 and $\beta(\Delta x)$ is different. Therefore, a two-parameter nonlinear optimization was performed at each lateral position to find $A(\Delta x)$ and $\beta(\Delta x)$, while keeping k fixed

$$\{A(\Delta x), \beta(\Delta x)\} = \underset{A, \beta}{\operatorname{argmin}} [|\hat{S}(f, \Delta x)| - Af^{k_0-1} \cdot \exp(-f\beta)]^2. \quad (12)$$

In the latter equation, $A(\Delta x)$ accounts for frequency-independent amplitude changes. The curve $\beta(\Delta x)$ was then fitted to a straight line over a length L , starting at x_0 , to obtain the attenuation coefficient through (8). To illustrate the method, the values of $\beta(\Delta x)/(k_0 - 1)$ obtained for the 0% oil phantom and their inverse (the peak frequency) are represented in Fig. 3, together with model predictions obtained for the fitted attenuation coefficient. It can be observed that the model, based on a linear attenuation hypothesis and a gamma-distributed spectrum, accurately describes the variation in the frequency content of the shear wave.

The influence of the averaging height h and fitting length L on the precision of the estimations was investigated. The standard deviation of the linear fit was computed for various lengths L (i.e., various number n of points included into the fit) as

$$\sigma(L, h) = \sqrt{\frac{1}{n-2} \frac{\sum_{i=1}^n (f_{p,i} - \tilde{f}_{p,i})^2}{(\Delta x_i - \bar{\Delta x})}} \quad (13)$$

and for various averaging depths h . In (13), $\tilde{f}_{p,i}$ are the peak frequencies predicted by the linear relation, and $\bar{\Delta x} = (1/n) \sum \Delta x$. In all cases, the left boundary of the region of interest (ROI) was set to 5 mm away from the push location, and centered at a depth $z = 25$ mm (position of the central push).

Finally, the influence of the distance x_0 between the left boundary of the ROI and the push position was also investigated. As the shape parameter k_0 is estimated once for all x_0 , it was important to investigate the influence of this parameter on the estimated attenuation coefficient. For that purpose, $\alpha_0(x_0)$ was computed for the three phantoms for x_0 ranging from 4 to 9 mm.

C. Plane-Wave Measurements

For validation purposes, the attenuation was measured in the three *in vitro* phantoms using the plane-wave polarization method, as in [6]. The large plate inserted in the phantom was driven by a mini-shaker (type 4810, Brüel and Kjær, Nærum, Denmark) connected to a waveform generator (33250A, Agilent Technologies, Santa Clara, CA, USA) and to a power amplifier (type 2706, Brüel and Kjær) (Fig. 1). The excitation signals were eight-period Blackman-windowed sinusoids at a central frequency ranging from 200 to 1300 Hz with 100-Hz increments. The amplitude of the excitation was 15 V peak to peak. The maximum frequency for which the results were exploitable varied depending on the oil concentration.

The same US probe used for radiation force measurements tracked planar shear waves at a 4 kHz frame rate for 60 ms, immediately after the excitation of the plate. Particle velocity fields were obtained using the same cross-correlation algorithm. The time signals were windowed in time to keep only forward propagating waves, and a Fourier transform was applied. The phase and amplitude of the waves as a function of propagation distance were extracted at the central frequency of each excitation signal. Phase velocity and attenuation were estimated from a linear fit of the phase and log amplitude, respectively [6]. Uncertainties on these quantities were estimated from the residuals of the linear fit. The absence of higher harmonics in the recorded wave field (Fig. 4) confirmed the linear regime of propagation for the shear waves generated by the vibrating plate. Nonlinear effects could have led to an overestimation of the attenuation at the excitation frequency due to energy transfer from the fundamental frequency to higher harmonics [37]. The plane-wave (reference) and frequency-shift measurements were performed one just after the other for the exact same position of the probe on the samples (Fig. 1). The processing for the plane-wave method was performed at a depth of 25 mm, corresponding to the depth of the central push of the tested method.

This plane-wave method has been recently compared with conventional rheometry [38], which is a gold standard for the viscoelastic characterization of soft materials. The shear-wave velocity and attenuation values extrapolated from the low-frequency rheometer measurements were highly correlated ($r > 0.86$) to the results of the plane-wave method, justifying its use as a reference method here.

D. Tests With *Ex Vivo* Porcine Livers

The frequency-shift method was applied to two freshly excised porcine livers. The same acquisition parameters as for phantom experiments were used. For each liver, a few arbitrary positioning of the probe on its surface were tested, and the data analysis was done for the position where the

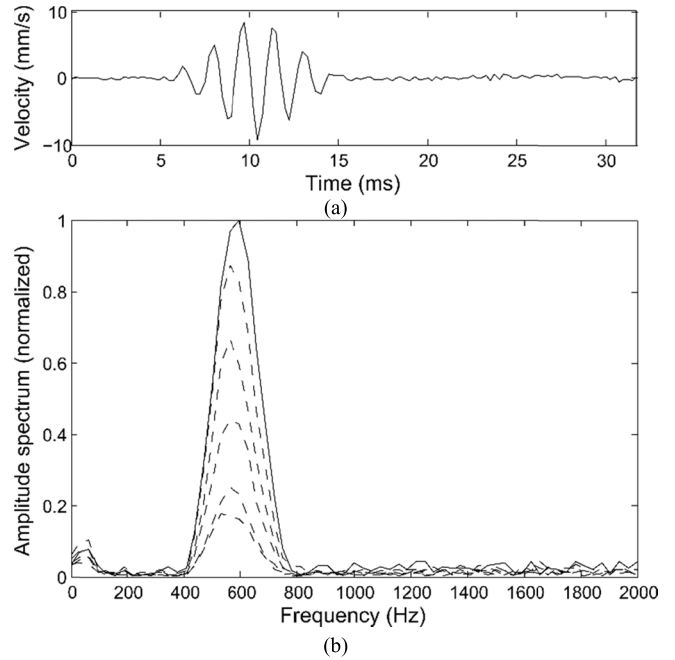


Fig. 4. (a) Time profile of the particle velocity field for shear waves generated by the vibrating plate, recorded about 20 mm away from the plate, for a 600-Hz excitation frequency. (b) Corresponding amplitude spectrum (solid line) and spectra obtained at increasing distances from the plate (dashed lines). No higher harmonics are visible in the spectra, indicating a linear propagation regime.

best displacement field was obtained (i.e., a well-defined propagating wavefront). The ROI for the data processing was placed 5 mm away from the pushing line. The height h was set to 10 mm, according to the analysis of this parameter made on the phantoms (see Section IV), and the optimal fitting length L was determined independently for each sample as the length minimizing (13), with the constraint $L < 10$ mm.

E. Tests on the *In Vivo* Biceps Muscle

For *in vivo* measurements of the *biceps brachii* attenuation, the ultrafast sequence was modified to introduce compounding angles [39]. This was necessary to reduce sidelobe artifacts and to improve the signal-to-noise ratio of the estimated shear-wave velocity field. Five angles separated by 2° (-4° , -2° , 0° , 2° , and 4°) were successively insonified at a repetition frequency of 12 500 Hz. The images obtained from the five angles were summed before motion estimation (coherent compounding), to get a 2500-Hz effective frame rate. The same motion estimation algorithm described earlier was used, and the particle velocity field was averaged over ten successive acquisitions. The push duration was increased to 200 μ s to enhance the displacement field, and the pushes were focused at 15, 20, and 25 mm. The ROI for the processing was placed 6 mm away from the pushing line. The height h was 10 mm and the optimal fitting length L was determined independently for each measurement, as for the *ex vivo* liver samples (Section III-D).

Measurements were performed on the biceps of a healthy volunteer (27-year-old male), with the muscle at rest and the elbow forming a 90° angle. A signed informed consent

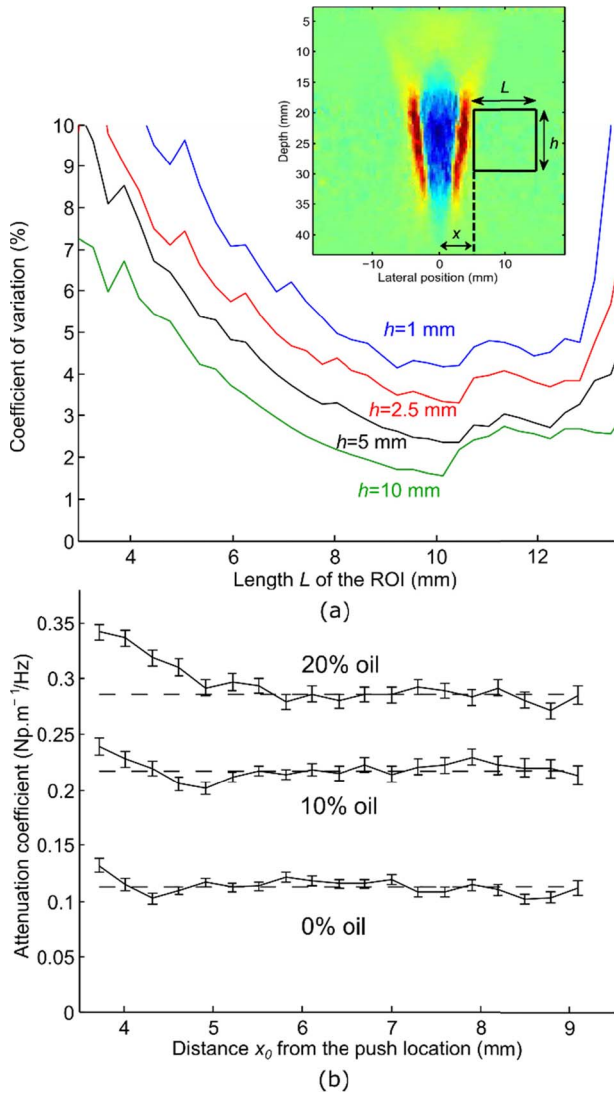


Fig. 5. (a) Influence of the ROI length L and height h on the coefficient of variation of the estimated attenuation coefficients for the 0% oil phantom. Minimum variation was obtained for a $10 \times 10 \text{ mm}^2$ ROI. (b) Attenuation coefficient for varying lateral position x_0 of the ROI and mean values (dashed lines) for the three tested phantoms with 0%–20% castor oil. The estimation weakly depends on x_0 .

approved by the Ethical Committee of the University of Montreal Hospital Research Center was obtained. The measurements were performed along (probe parallel to the arm) and across the muscle fibers (probe perpendicular to the arm). For both orientations, the whole measurement was repeated five times with intermediate repositioning of the probe. Shear waves were generated in the center of the ultrasonic probe, and the attenuation was evaluated independently on both sides of the pushes, yielding a total of $5 \times 2 = 10$ measurements for each muscle orientation to evaluate the repeatability.

IV. RESULTS

The results of the analysis of the ROI size and position are summarized in Fig. 5. As seen in Fig. 5(a), for the 0% oil phantom, increasing the depth of averaging h reduces the coefficient of variation (i.e., $\text{mean} \times 100 / \text{standard deviation}$) of the estimated attenuation coefficients. Increasing the length

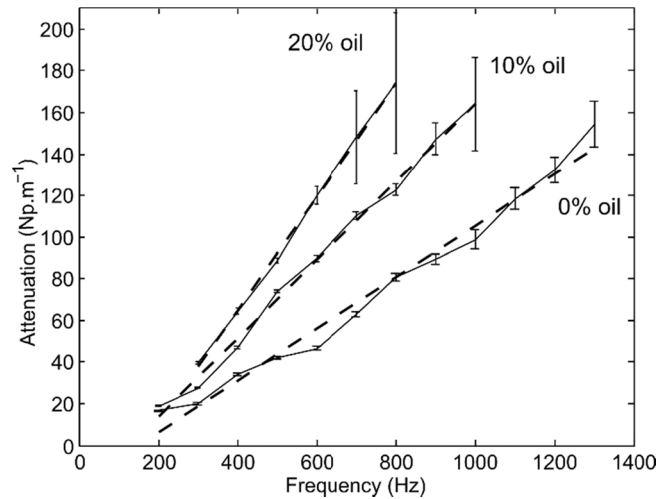


Fig. 6. Frequency-dependent attenuation measured with the plane-wave reference method for the three agar–gelatin–oil phantoms. Fitting to a linear model (dashed lines) yields the attenuation coefficient α_0 .

of the linear fit L also reduces this coefficient of variability, but only up to about 10 mm. Based on these observations, we fixed the size of the ROI to $10 \times 10 \text{ mm}^2$ for the phantom study. It implies that we assumed the tested material to be homogeneous in that ROI. As shown in Fig. 5(b), the estimated attenuation coefficients weakly depend on the ROI position for $x_0 > 5 \text{ mm}$ (variations of about 5%), which confirms that the rate parameter k_0 does not vary with the propagating distance. The results obtained for $x_0 < 5 \text{ mm}$ were biased because the complete temporal waveform was not available close to the radiation pressure source, due to a $500\text{-}\mu\text{s}$ waiting time between the last push and the beginning of the imaging sequence. This delay could not be reduced because the imaging sequence cannot start until the echoes of the pushing beam are fully dissipated. The shear-wave velocity in the phantoms was about 4 m/s.

The attenuation as a function of frequency for the three *in vitro* phantoms, obtained with the plane-wave reference vibration method, is plotted in Fig. 6. It can be observed that the frequency dependence of the attenuation was linear in the measured frequency band ($r > 0.99$, $p < 10^{-5}$). The attenuation coefficients, extracted from straight line fittings of the results, were 0.122 ± 0.006 , 0.188 ± 0.002 , and $0.273 \pm 0.008 \text{ Np m}^{-1}/\text{Hz}$ for 0%, 10%, and 20% oil concentrations, respectively. The uncertainties were estimated from the standard deviations of the linear fit. The attenuation coefficients obtained with the proposed frequency-shift method for $x_0 = 5 \text{ mm}$ were 0.117 ± 0.004 , 0.202 ± 0.005 , and $0.292 \pm 0.007 \text{ Np m}^{-1}/\text{Hz}$. The results from the two methods are compared in Fig. 7. Good agreements can be observed, with relative differences of 4%, 7%, and 7% depending on the oil concentration. These differences are only slightly larger than the estimated precisions of both methods. The correlation coefficient between the results of the two methods is $r > 0.99$ ($p < 0.05$).

The attenuation coefficients measured for the two *ex vivo* porcine livers are 0.79 ± 0.02 and $1.35 \pm 0.03 \text{ Np m}^{-1}/\text{Hz}$. The uncertainty comes from the standard deviation of the linear fit

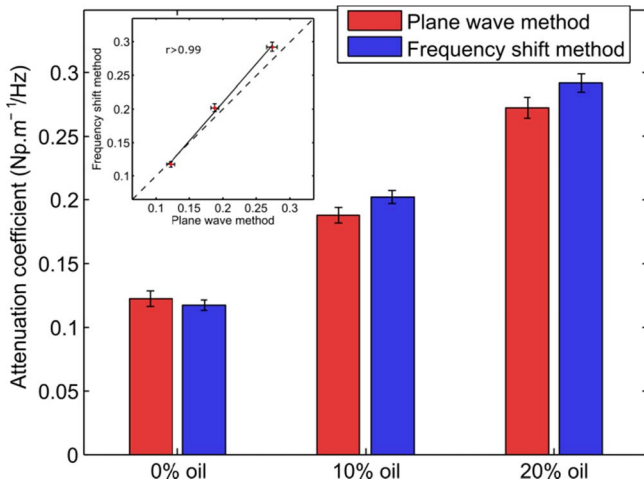


Fig. 7. Attenuation coefficients in the three phantoms measured with the plane-wave reference method and with the tested frequency-shift method. The two methods are in good agreement.

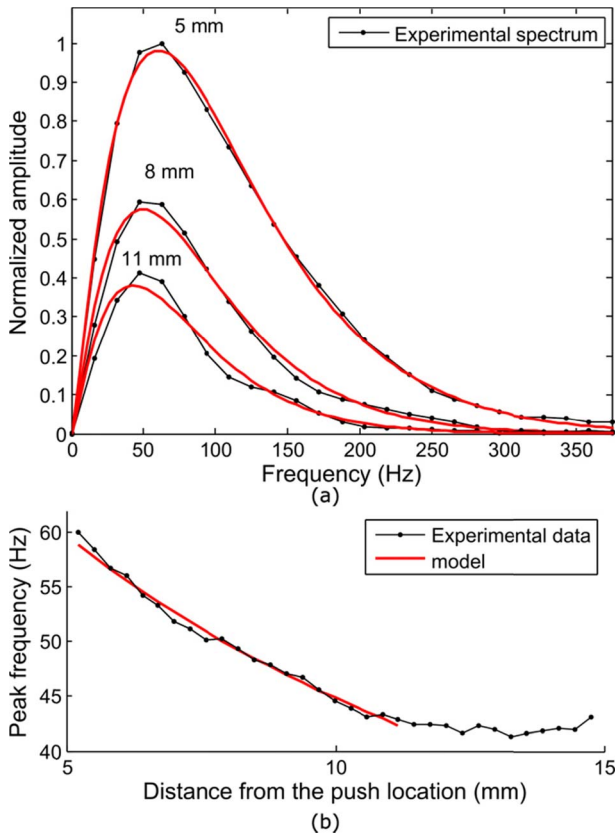


Fig. 8. Results for one of the porcine liver samples. (a) Three representative amplitude spectra of the propagating shear wave. (b) Peak frequency of the gamma-shaped spectra as a function of the propagation distance and prediction of the model after fitting for the attenuation coefficient. Eleven millimeters away from the pushing line, the peak frequency estimation becomes dominated by noise.

of the rate parameter β , as obtained from the residuals of the least-square fit. As an example, the spectrum and peak frequency as a function of the distance for one of the liver samples (at $1.35 \text{ Np m}^{-1}/\text{Hz}$) are plotted in Fig. 8. The gamma distribution provides a good fit to the measured amplitude spectrum: the correlation coefficients r between the data and

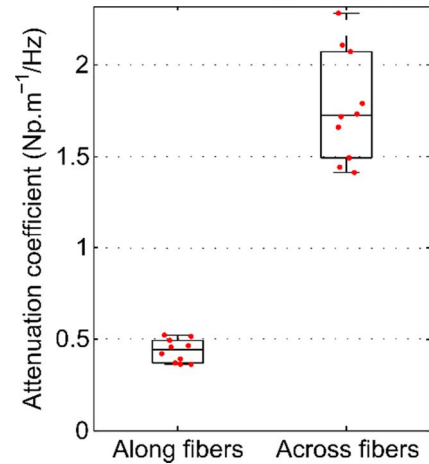


Fig. 9. Results of ten successive measurements on the *biceps brachii* muscle of a healthy volunteer *in vivo*. The boxes show the median, and the first and third quartiles.

the model were 0.99, 0.98, and 0.94 for the three pictured curves. The optimal fitting length L was 6.3 mm. Because the attenuation was stronger than in the phantoms, the estimated central frequency after 11 mm was dominated by noise and stopped decreasing [Fig. 8(b)]. At that distance, the peak particle velocity was small: about 0.5 mm/s, for a standard deviation of the field of about 0.07 mm/s.

The attenuation coefficients measured for ten successive experiments in the *biceps brachii* are plotted in Fig. 9. The mean value and standard deviation of the attenuation coefficients are $0.43 \pm 0.06 \text{ Np m}^{-1}/\text{Hz}$ along the tissue fibers and $1.77 \pm 0.30 \text{ Np m}^{-1}/\text{Hz}$ across them. The repeatability was therefore about 15% for both cases. This included not only measurement errors but also potential effects of tissue inhomogeneity, as the probe was moved and approximately repositioned at the same location between measurements. A strong anisotropy was observed, with an anisotropy ratio of 4, indicating that the attenuation was much stronger across the tissue fibers. The spectrum and peak frequency as a function of the propagation distance for one of the *in vivo* experiments are plotted in Fig. 10. Overall, good agreement is observed between the proposed model and experimental data (r of 0.99, 0.98, and 0.96 along the fibers, and 0.99, 0.96, and 0.79 across the fibers for the pictured curves). Across the tissue fibers, the mean optimal length L over the ten experiments was 6.5 mm. It was indeed observed that the peak frequency could not be accurately estimated after about 12 mm of propagation [Fig. 10(b)]. At that distance, the peak particle velocity was about 0.3 mm/s, while the standard deviation of the field was about 0.05 mm/s.

V. DISCUSSION

A gamma distribution was used to describe the shear-wave amplitude spectrum because it is a simple function that depends only on two scalar parameters that can be easily related to sound physical quantities (mean and peak frequencies). Another advantage of this model is its flexibility to relate its parameters to the linear attenuation hypothesis. Indeed, the shear wave keeps a gamma-distributed spectrum

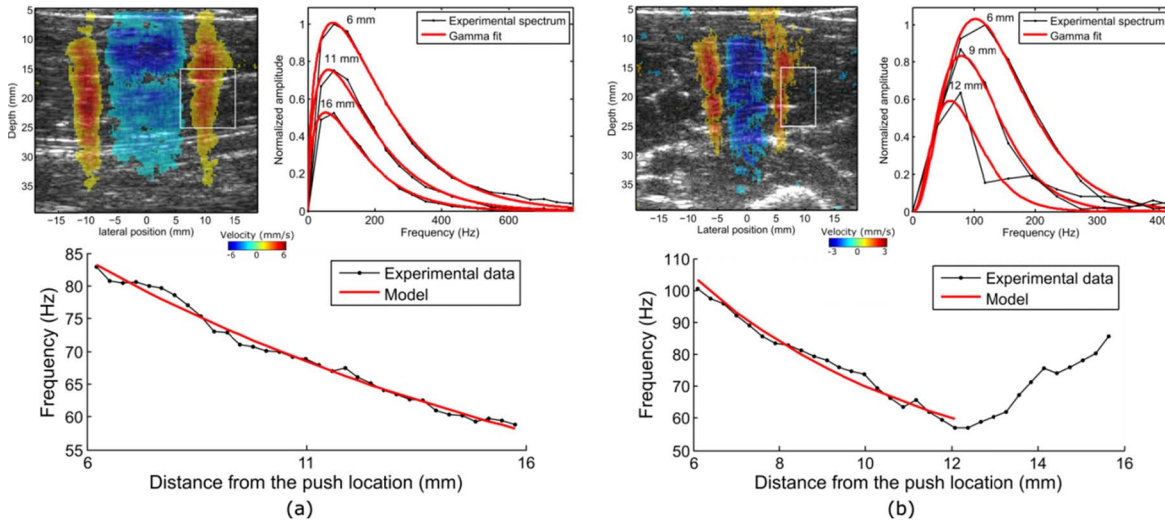


Fig. 10. Shear-wave fields superposed on B-mode images, amplitude spectra of the shear waves, and peak frequency versus propagation distance for an *in vivo biceps brachii* muscle measured (a) along and (b) across the tissue fibers. Both wave fields are represented about 5 ms after the acoustic radiation pushes. For propagation across the tissue fibers, the peak frequency estimated with a gamma fit of the spectrum starts to be dominated by noise at about 12 mm away from the push location.

during propagation in the attenuating medium, with one parameter being constant and the other linearly varying with the propagation distance. This property allowed a straightforward estimation of the attenuation coefficient. Finally, and most importantly, the gamma model provided an excellent fit to amplitude spectra, as observed in Fig. 2 for phantoms and Figs. 8 and 10 for biological tissues. This observation was quantitatively confirmed by the high correlation coefficients obtained between the data and the model.

Processing was here performed on the particle velocity fields, since these are directly obtained from correlation of successive US frames. The displacement and velocity fields are related by a derivation operation in the time domain and therefore related by a $j\omega$ factor in the frequency domain. It implies that if the particle velocity amplitude spectrum is gamma distributed, then the displacement amplitude spectrum is also gamma distributed with the same rate parameter β_0 . The method should therefore be applicable to the displacement field as well, although the dominant low-frequency components in the displacement field may affect the sensitivity. This aspect was not investigated in this paper.

Frequency-dependent wave attenuation is commonly described by a power law model

$$\alpha(f) = a_0 f^\gamma \quad (14)$$

in a wide variety of materials and over a wide frequency range, with an exponent $0 < \gamma < 2$ (see [40] and the references therein). In particular, the linear case $\gamma = 1$ is very popular in seismology [41]. It is the simplest possible model, while still being consistent with the physical requirement of causality and able to accurately describe experimental data. In this paper, we hypothesized that the linear attenuation model could also be appropriate for shear-wave attenuation in soft tissues, in the frequency range of radiation force elastography.

Previously published data indirectly support this linear frequency-dependent hypothesis. On the attenuation curves obtained in [6] for an agar/gelatin phantom and *ex vivo* beef

muscle using the plane-wave method [6, Figs. 6 and 8], one can see that a simple linear model would have provided a fit that is at least as good as the Voigt model used by the authors. Urban and Greenleaf [42] used a power law model (14) to fit the wave attenuation measured on a bovine *ex vivo* muscle and obtained exponents of 1.18 and 0.85, along and across the muscle, respectively. These exponents are relatively close to 1, and indicate that a simpler linear model might have been sufficient to explain the tissue attenuation.

The linear attenuation hypothesis is also well supported *a posteriori* by our data. In phantoms, the plane-wave measurements clearly revealed the linear dependence of the attenuation in the investigated frequency band (Fig. 6). For the *ex vivo* and *in vivo* tissue study, we have indirect evidence: the wave spectrum variations were well described by a gamma distribution whose shape parameter was constant and rate parameter was a linear function of the propagation distance, as predicted by the model. We cannot, however, affirm that the linear attenuation law will be accurate for other types of phantoms or tissues, or even for liver and muscle tissues affected by pathologies. In US imaging, the optimal exponent of the power law for compressional wave attenuation differs from unity in some tissues, and the frequency-shift equation for Gaussian spectrum has therefore been generalized to account for nonlinear (power law) attenuation [43]. Future investigations might prove necessary to perform a similar generalization for the present method, although the simplicity will likely be affected. This might be achieved using a generalized gamma distribution, which takes as a third parameter p the power applied to the frequency term in the decreasing exponential ($p = 1$ for the gamma distribution).

In the phantom experiments, good agreement was obtained between the reference plane-wave vibration method and the proposed frequency-shift method, establishing the accuracy of the proposed approach. As expected, the attenuation coefficient was found to increase with the castor oil concentration. Nevertheless, the largest attenuation observed in phantoms was

still small compared with the attenuation coefficients observed in liver and muscle tissues. This suggests that although the proposed fabrication method allowed more realistic phantoms, the adjunction of oil in the proportions used here still do not perfectly represent the viscoelasticity of biological tissues. Acrylamide hydrogels have also been used to prepare viscoelastic phantoms [38], [44], and may allow obtaining a higher attenuation.

The *in vivo* experiments on the biceps muscle demonstrated the good reproducibility of the method. For both orientations of the probe (across and along tissue fibers), a standard deviation of about 15% was obtained over ten repeated measurements with intermediate probe repositioning. Using MR elastography, [11] measured a mean attenuation of 38.1 Np/m at 90 Hz in the *vastus medialis* muscle of healthy individuals, compared with 55.6 Np/m for patients suffering of myositis and 65.1 Np/m for patients with hyperthyroid myopathy (46% and 71% increases, respectively). Our method should therefore be able to discriminate healthy and diseased tissues in such context. The attenuation coefficient of 0.43 ± 0.06 Np m^{-1}/Hz measured here along the tissue fibers leads to an attenuation of 39 ± 5 Np/m at 90 Hz, in good quantitative agreement with the value of 38.1 Np/m measured using MR elastography in healthy individuals [11]. Finally, the strong anisotropy observed in the attenuation coefficient along and across tissue fibers (anisotropy ratio of 4) is consistent with the qualitative observations of attenuation reported in [14] for the *biceps brachii* of three volunteers.

The attenuation measurement method introduced here relies on shear waves generated by a line of radiation force pushes. This kind of pushing sequence is already available in several commercial clinical elastography systems and used in clinical settings. The imaging sequence, whether it uses compounding angles or not, is also conventional. Only an original data processing algorithm, focusing on variations in the frequency content of the wave, was introduced. Therefore, it is believed that the frequency-shift method could be simply implemented and used in clinical systems. Moreover, the processing is rather fast. The most demanding operation is certainly the nonlinear fitting of the spectrum by a gamma distribution at each lateral position. For the ROI size used in this paper, and on a desktop computer, the processing time was of the order of 1 s. The results can then be displayed almost immediately after the shear-wave excitation.

Applying attenuation measurement methods based on diffraction correction [17], [18] to anisotropic materials such as muscles would be less practical than with the present method. Indeed, due to anisotropy, the shear wavefront would be elliptical with a different decrease rate in each direction. If the anisotropy is measured beforehand, it may be possible to predict the shape of the wavefront using numerical simulations [23], [24] and to correct for the diffraction effects. This would, however, be difficult to implement in a clinical context. Note that, for the present method, we assumed the propagation directions to be perfectly orthogonal or parallel to the muscle fibers. For other propagation directions and/or arbitrary orientation of the shear-wave source, the attenuation observed in the imaging plane would likely be affected by

the coupling between the distinct propagation modes existing in anisotropic materials. This could be investigated through numerical simulations in future work.

The ROI size and position, and then the estimated attenuation coefficient, depend on three parameters: the averaging depth h , the length L , and the lateral distance from the push location x_0 . It was found on phantoms that increasing h up to 10 mm decreased the variance of the estimation; this value was used for all subsequent experiments. Increasing even further h would hardly make sense, as the depth of the ROI would then exceed the depth of the pushing line. The length L was determined in each case from an analysis of the goodness of fit of the linear fitting of the peak frequency. It is an automated procedure. The optimal length was found to be between 10 (low attenuation) and 6 mm (high attenuation). Finally, it was found that the location x_0 has a weak influence on the estimated attenuation, as long as it is large enough (>5 mm here) for the temporal waveform to be recorded entirely at x_0 . Closer to the source, near-field effects may also influence the results, as the model developed in Section II considers a propagating wave, with no source terms. Media with shear-wave velocity higher than 4 m/s may, however, require considering a larger x_0 , as the wave would travel on a larger distance during the 500- μ s waiting time at the beginning of the imaging sequence.

The attenuation estimation method presented here can be combined to a shear-wave dispersion measurement method giving wave velocity versus frequency, such as [14], to provide the shear viscoelastic modulus (storage and loss moduli) without relying on an assumed rheological model. The theory relating frequency-dependent shear-wave velocity and attenuation to the storage and loss moduli can be found elsewhere (see [10], [38]). However, as already discussed, the present method is limited to linear frequency-dependent attenuation. Regarding that particular point, the present method is less general than methods relying on geometrical diffraction correction [17], [18], which estimate attenuation at each frequency independently.

A final remark is that the present method was developed for applications to tissues that can be considered macroscopically homogeneous and for which a single estimate is obtained from a selected ROI. Depending on the probe orientation, we nevertheless showed that the proposed method is of interest to study tissue anisotropy. Other applications in elastography are interested in the spatial variations of mechanical parameters (e.g., breast cancer or thyroid nodule diagnosis). It would therefore be of interest to develop a tissue attenuation mapping method based on the frequency-shift equation. This would be feasible by studying different ROIs along the acoustic radiation pressure pushes' path. Moreover, the propagation was here assumed to be strictly 1-D along the lateral direction of the probe. This is a common assumption for the shear-wave generation configuration used here [14], [20]. Recently proposed excitation methods relying on multiple and/or steered push beams [36], [45], as well as wave refraction and reflection occurring in heterogeneous materials might require to generalize our approach to a 2-D analysis or to use directional filtering.

VI. CONCLUSION

Shear-wave elastography has been used for years to measure shear-wave speed in soft tissues and to deduce their elasticity. In contrast, shear-wave attenuation, which is primarily related to the viscous behavior of tissues, has been barely studied because of methodological difficulties. In this paper, we proposed a new method to measure the attenuation of shear waves generated by radiation force pushes in soft tissues. This method, inspired by the frequency-shift method used in US imaging and seismology, is based on the shift of the amplitude spectrum of the wave toward low frequencies during propagation. This shift is due to stronger attenuation of the high-frequency components of the spectrum. The accuracy of the method was assessed using *in vitro* phantoms whose viscosity, and hence attenuation, was varied by the addition of oil in the agar and gelatin mixture. Applicability to biological tissues was demonstrated on *ex vivo* porcine samples and *in vivo* on human muscle tissues.

Contrary to previously proposed approach based on wave amplitude or frequency–wavenumber analysis, the frequency-shift method does not require to correct for the geometrical spreading of the wave. Consequently, it may be easier to apply in some contexts, such as applications to anisotropic tissues.

REFERENCES

- [1] A. Sarvazyan *et al.*, “Biophysical bases of elasticity imaging,” in *Acoustical Imaging*, vol. 21. New York, NY, USA: Springer, 1995, pp. 223–240.
- [2] A. P. Sarvazyan, O. V. Rudenko, S. D. Swanson, J. B. Fowlkes, and S. Y. Emelianov, “Shear wave elasticity imaging: A new ultrasonic technology of medical diagnostics,” *Ultrasound Med. Biol.*, vol. 24, no. 9, pp. 1419–1435, 1998.
- [3] W. A. Berg *et al.*, “Shear-wave elastography improves the specificity of breast US: The BE1 multinational study of 939 masses,” *Radiology*, vol. 262, no. 2, pp. 435–449, Feb. 2012.
- [4] M. L. Palmeri *et al.*, “Noninvasive evaluation of hepatic fibrosis using acoustic radiation force-based shear stiffness in patients with nonalcoholic fatty liver disease,” *J. Hepatol.*, vol. 55, no. 3, pp. 666–672, Sep. 2011.
- [5] T. Gallot, S. Catheline, P. Roux, J. Brum, N. Benech, and C. Negreira, “Passive elastography: Shear-wave tomography from physiological-noise correlation in soft tissues,” *IEEE Trans. Ultrason., Ferroelect., Freq. Control*, vol. 58, no. 6, pp. 1122–1126, Jun. 2011.
- [6] S. Catheline *et al.*, “Measurement of viscoelastic properties of homogeneous soft solid using transient elastography: An inverse problem approach,” *J. Acoust. Soc. Amer.*, vol. 116, no. 6, pp. 3734–3741, 2004.
- [7] M. Fatemi and J. F. Greenleaf, “Ultrasound-stimulated vibro-acoustic spectrography,” *Science*, vol. 280, pp. 82–85, Apr. 1998.
- [8] K. R. Nightingale, M. L. Palmeri, R. W. Nightingale, and G. E. Trahey, “On the feasibility of remote palpation using acoustic radiation force,” *J. Acoust. Soc. Amer.*, vol. 110, pp. 625–634, Jul. 2001.
- [9] J. Bercoff, M. Tanter, and M. Fink, “Supersonic shear imaging: A new technique for soft tissue elasticity mapping,” *IEEE Trans. Ultrason., Ferroelect., Freq. Control*, vol. 51, no. 4, pp. 396–409, Apr. 2004.
- [10] R. S. Lakes, *Viscoelastic Materials*. Cambridge, U.K.: Cambridge Univ. Press, 2009.
- [11] Z. J. Domire, M. B. McCullough, Q. Chen, and K.-N. An, “Wave attenuation as a measure of muscle quality as measured by magnetic resonance elastography: Initial results,” *J. Biomech.*, vol. 42, no. 4, pp. 537–540, Mar. 2009.
- [12] P. Garteiser *et al.*, “MR elastography of liver tumours: Value of viscoelastic properties for tumour characterisation,” *Eur. Radiol.*, vol. 22, no. 10, pp. 2169–2177, Oct. 2012.
- [13] Y. Qiu, M. Sridhar, J. K. Tsou, K. K. Lindfors, and M. F. Insana, “Ultrasonic viscoelasticity imaging of nonpalpable breast tumors: Preliminary results,” *Acad. Radiol.*, vol. 15, no. 12, pp. 1526–1533, Dec. 2008.
- [14] T. Deffieux, G. Montaldo, M. L. Tanter, and M. Fink, “Shear wave spectroscopy for *in vivo* quantification of human soft tissues viscoelasticity,” *IEEE Trans. Med. Imag.*, vol. 28, no. 3, pp. 313–322, Mar. 2009.
- [15] M. Tanter *et al.*, “Quantitative assessment of breast lesion viscoelasticity: Initial clinical results using supersonic shear imaging,” *Ultrasound Med. Biol.*, vol. 34, no. 9, pp. 1373–1386, Sep. 2008.
- [16] S. Chen, M. Fatemi, and J. F. Greenleaf, “Quantifying elasticity and viscosity from measurement of shear wave speed dispersion,” *J. Acoust. Soc. Amer.*, vol. 115, no. 6, pp. 2781–2785, 2004.
- [17] I. Z. Nenadic *et al.*, “Application of attenuation measuring ultrasound shearwave elastography in 8 post-transplant liver patients,” in *Proc. IEEE Int. Ultrason. Symp. (IUS)*, Chicago, IL, USA, Sep. 2014, pp. 987–990.
- [18] S. Kazemirad, S. Bernard, S. Hybois, A. Tang, and G. Cloutier, “Ultrasound shear wave viscoelastography: Model-independent quantification of the complex shear modulus,” *IEEE Trans. Ultrason., Ferroelect., Freq. Control*, vol. 63, no. 9, pp. 1399–1408, Sep. 2016.
- [19] N. C. Rouze, M. L. Palmeri, and K. R. Nightingale, “An analytic, Fourier domain description of shear wave propagation in a viscoelastic medium using asymmetric Gaussian sources,” *J. Acoust. Soc. Amer.*, vol. 138, no. 2, pp. 1012–1022, 2015.
- [20] J.-L. Gennisson, T. Deffieux, E. Macé, G. Montaldo, M. Fink, and M. L. Tanter, “Viscoelastic and anisotropic mechanical properties of *in vivo* muscle tissue assessed by supersonic shear imaging,” *Ultrasound Med. Biol.*, vol. 36, no. 5, pp. 789–801, 2010.
- [21] J. Brum, M. Bernal, J. L. Gennisson, and M. Tanter, “*In vivo* evaluation of the elastic anisotropy of the human Achilles tendon using shear wave dispersion analysis,” *Phys. Med. Biol.*, vol. 59, no. 3, pp. 505–523, 2014.
- [22] J.-L. Gennisson, N. Grenier, C. Combe, and M. Tanter, “Supersonic shear wave elastography of *in vivo* pig kidney: Influence of blood pressure, urinary pressure and tissue anisotropy,” *Ultrasound Med. Biol.*, vol. 38, no. 9, pp. 1559–1567, 2012.
- [23] N. C. Rouze, M. H. Wang, M. L. Palmeri, and K. R. Nightingale, “Finite element modeling of impulsive excitation and shear wave propagation in an incompressible, transversely isotropic medium,” *J. Biomech.*, vol. 46, no. 16, pp. 2761–2768, 2013.
- [24] S. Chatelin, J.-L. Gennisson, M. Bernal, M. Tanter, and M. Pernot, “Modelling the impulse diffraction field of shear waves in transverse isotropic viscoelastic medium,” *Phys. Med. Biol.*, vol. 60, no. 9, pp. 3639–3654, 2015.
- [25] K. A. Dines and A. C. Kak, “Ultrasonic attenuation tomography of soft tissues,” *Ultrason. Imag.*, vol. 1, no. 1, pp. 16–33, 1979.
- [26] M. Fink, F. Hottier, and J. F. Cardoso, “Ultrasonic signal processing for *in vivo* attenuation measurement: Short time Fourier analysis,” *Ultrason. Imag.*, vol. 5, no. 2, pp. 117–135, 1983.
- [27] R. Kuc, M. Schwartz, and L. V. Micsky, “Parametric estimation of the acoustic attenuation coefficient slope for soft tissue,” in *Proc. IEEE Ultrason. Symp.*, Annapolis, MD, USA, Sep./Oct. 1976, pp. 44–47.
- [28] T. A. Bigelow and Y. Labyed, “Attenuation Compensation and Estimation,” in *Quantitative Ultrasound in Soft Tissues*, J. Mamou and M. L. Oelze, Eds. New York, NY, USA: Springer, 2013, pp. 71–93.
- [29] Y. Quan and J. M. Harris, “Seismic attenuation tomography using the frequency shift method,” *Geophysics*, vol. 62, no. 3, pp. 895–905, 1997.
- [30] L. Liu, J. W. Lane, and Y. Quan, “Radar attenuation tomography using the centroid frequency downshift method,” *J. Appl. Geophys.*, vol. 40, pp. 105–116, Oct. 1998.
- [31] L. Allard, G. Soulez, B. Chayer, Z. Qin, D. Roy, and G. Cloutier, “A multimodality vascular imaging phantom of an abdominal aortic aneurysm with a visible thrombus,” *Med. Phys.*, vol. 40, no. 6, pp. 063701-1–063701-10, 2013.
- [32] A. Ouared, E. Montagnon, S. Kazemirad, L. Gaboury, A. Robidoux, and G. Cloutier, “Frequency adaptation for enhanced radiation force amplitude in dynamic elastography,” *IEEE Trans. Ultrason., Ferroelect., Freq. Control*, vol. 62, no. 8, pp. 1453–1466, Aug. 2015.
- [33] D. Garcia, L. Le Tarnec, S. Muth, E. Montagnon, J. Porée, and G. Cloutier, “Stolt’s f-k migration for plane wave ultrasound imaging,” *IEEE Trans. Ultrason., Ferroelect., Freq. Control*, vol. 60, no. 9, pp. 1853–1867, Sep. 2013.
- [34] J. Luo and E. E. Konofagou, “A fast normalized cross-correlation calculation method for motion estimation,” *IEEE Trans. Ultrason., Ferroelect., Freq. Control*, vol. 57, no. 6, pp. 1347–1357, Jun. 2010.
- [35] T. Deffieux, J.-L. Gennisson, J. Bercoff, and M. Tanter, “On the effects of reflected waves in transient shear wave elastography,” *IEEE Trans. Ultrason., Ferroelect., Freq. Control*, vol. 58, no. 10, pp. 2032–2035, Oct. 2011.

- [36] P. Song, A. Manduca, H. Zhao, M. W. Urban, J. F. Greenleaf, and S. Chen, "Fast shear compounding using robust 2-D shear wave speed calculation and multi-directional filtering," *Ultrasound Med. Biol.*, vol. 40, no. 6, pp. 1343–1355, 2014.
- [37] S. Catheline, J.-L. Gennisson, M. Tanter, and M. Fink, "Observation of shock transverse waves in elastic media," *Phys. Rev. Lett.*, vol. 91, no. 16, pp. 164301-1–164301-4, Oct. 2003.
- [38] J.-L. Gennisson, A. Marcellan, A. Dizeux, and M. Tanter, "Rheology over five orders of magnitude in model hydrogels: Agreement between strain-controlled rheometry, transient elastography, and supersonic shear wave imaging," *IEEE Trans. Ultrason., Ferroelect., Freq. Control*, vol. 61, no. 6, pp. 946–954, Jun. 2014.
- [39] G. Montaldo, M. Tanter, J. Bercoff, N. Benech, and M. Fink, "Coherent plane-wave compounding for very high frame rate ultrasonography and transient elastography," *IEEE Trans. Ultrason., Ferroelect., Freq. Control*, vol. 56, no. 3, pp. 489–506, Mar. 2009.
- [40] T. L. Szabo, "Time domain wave equations for lossy media obeying a frequency power law," *J. Acoust. Soc. Amer.*, vol. 96, no. 1, pp. 491–500, 1994.
- [41] K. Aki and P. G. Richards, *Quantitative Seismology*, vol. 1, 2nd ed. Sausalito, CA, USA: Univ. Science Books, 2002.
- [42] M. W. Urban and J. F. Greenleaf, "A Kramers–Kronig-based quality factor for shear wave propagation in soft tissue," *Phys. Med. Biol.*, vol. 54, no. 19, pp. 5919–5933, 2009.
- [43] J. Ophir and P. Jaeger, "Spectral shifts of ultrasonic propagation through media with nonlinear dispersive attenuation," *Ultrason. Imag.*, vol. 4, no. 3, pp. 282–289, 1982.
- [44] K. Kumar, M. E. Andrews, V. Jayashankar, A. K. Mishra, and S. Suresh, "Measurement of viscoelastic properties of polyacrylamide-based tissue-mimicking phantoms for ultrasound elastography applications," *IEEE Trans. Instrum. Meas.*, vol. 59, no. 5, pp. 1224–1232, May 2010.
- [45] A. Nabavizadeh, P. Song, S. Chen, J. F. Greenleaf, and M. W. Urban, "Multi-source and multi-directional shear wave generation with intersecting steered ultrasound push beams," *IEEE Trans. Ultrason., Ferroelect., Freq. Control*, vol. 62, no. 4, pp. 647–662, Apr. 2015.



Simon Bernard was born in Quimper, France, in 1988. He received the master's and Ph.D. degrees in physical acoustics from Université Pierre et Marie Curie, Paris, France, in 2011 and 2014, respectively. His Ph.D. work focused on the measurement of bone mechanical properties using ultrasound methods.

He was a Post-Doctoral Fellow with the Laboratory of Biorheology and Medical Ultrasonics, University of Montréal Hospital Research Center, Montréal, QC, Canada, where he was involved in shear wave elastography. His current research interests include ultrasound methods for material characterization, modeling of wave propagation and scattering, and inverse problem solutions.



Siavash Kazemirad received the B.Sc. degree in mechanical engineering from the Iran University of Science and Technology, Tehran, Iran, in 2006, the M.Sc. degree in mechanical engineering with a major in biomechanics, from the Sharif University of Technology, Tehran, in 2009, and the Ph.D. degree in mechanical engineering from McGill University, Montréal, QC, Canada, in 2013.

He was with the Biomechanics Research Laboratory, McGill University. In 2013, he joined the Laboratory of Biorheology and Medical Ultrasonics, University of Montreal Hospital Research Center, Montréal, as a Post-Doctoral Fellow. His current research interests include vibration and acoustics, wave propagation, ultrasound imaging, material characterization, and ultrasound elastography.



Guy Cloutier (S'89–M'90–SM'07) received the B.Eng. degree in electrical engineering from the Université du Québec à Trois-Rivières in 1984, and the M.Sc. and Ph.D. degrees in biomedical engineering from the École Polytechnique of Montreal in 1986 and 1990, respectively.

From 1990 to 1992, he was a Post-Doctoral Fellow with The Pennsylvania State University, State College, PA, USA, with Prof. K. K. Shung.

He is currently Director of the Laboratory of Biorheology and Medical Ultrasonics, University of Montreal Hospital Research Center, Montréal, QC, Canada, and a Professor with the Department of Radiology, Radio Oncology, and Nuclear Medicine, University of Montréal, Montréal. He is a member of the Institute of Biomedical Engineering at the University of Montréal. He was a recipient of the National Scientist Award of the Fonds de la Recherche en Santé du Québec from 2004 to 2009. He has authored more than 180 peer-reviewed articles in his research fields, holds 12 patents, and licensed three technologies. His current research interests include quantitative ultrasound imaging, quasi-static and dynamic ultrasound elastography, development of multiphysics imaging methods, and biomechanical modeling.

Dr. Cloutier was a member of the International Advisory Editorial Board of *Ultrasound in Medicine and Biology* for 15 years. He is currently a member of the Editorial Board of *Current Medical Imaging Reviews* and also an Associate Editor of the IEEE TRANSACTIONS ON ULTRASONICS, FERROELECTRIC, AND FREQUENCY CONTROL and an Invited Associate Editor of *Medical Physics*.